Penerbit Akademia Baru

Journal of Research in Nanoscience and Nanotechnology

Journal homepage:
http://akademiabaru.com/submit/index.php/jrnn/index
ISSN: 2773-6180

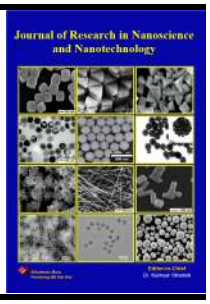

Perovskite Materials: From Fundamental Structure to Emerging Technologies

Kamyar Shameli [1,*], Aras Kartouzian[1]

TUM School of Natural Sciences & Catalysis Research Center, Technical University of Munich, 85748 Garching, Germany

* Correspondence: kamyar.shameli@tum.de

ABSTRACT

Perovskites, with the general formula ABX_3, constitute one of the most structurally versatile and functionally diverse families of crystalline materials. Their exceptional tolerance to compositional substitution enables the realization of a broad spectrum of physical phenomena, including ferroelectricity, colossal magnetoresistance, high-temperature superconductivity, and, in the case of metal halide perovskites, outstanding optoelectronic properties. This review provides a systematic examination of the crystallographic principles governing perovskite stability and distortion, the compositional landscape spanning oxide, halide, and double perovskite classes, and the synthetic methodologies employed to prepare single crystals, thin films, and nanocolloidal systems. Emphasis is placed on metal halide perovskites, whose remarkable charge-carrier transport characteristics, defect tolerance, and bandgap tunability have driven transformative advances in photovoltaics, light-emitting diodes, and radiation detection. The intrinsic instability of these materials under operational stressors moisture, oxygen, thermal exposure, and illumination is critically analyzed alongside contemporary mitigation strategies, including compositional engineering, interfacial passivation, and encapsulation. Finally, emerging research directions such as lead-free compositions, (chiral) hybrid perovskites, tandem device architectures, and integration with established semiconductor platforms are discussed, highlighting the trajectory toward commercial viability.

Keywords: Perovskite structure, Metal halide perovskite, Photovoltaics, Light-emitting diodes, Synthesis, Stability.

Received: 29 March 2026 **Revised: 13 April 2026** **Accepted: 21 April 2026** **Published: 30 April 2026**

1. Introduction

The term "perovskite" originates from the mineral calcium titanate ($CaTiO_3$), discovered by Gustav Rose in 1839 and subsequently named in honor of the Russian Mineralogist L. A. Perovski. Over the ensuing two centuries, this designation has expanded to encompass a vast class of compounds crystallizing in the eponymous structure a three dimensional framework of corner sharing BX_6 octahedra with the A cation occupying the resulting cuboctahedral cavities [1]. The generalized stoichiometry ABX_3 accommodates an exceptional range of ionic substitutions, enabling property tuning across orders of magnitude. Among mineral and non-metallic materials, whether in the form of nano/micro particles such as silver [2-4] and gold particles [5], or metal oxides like iron

oxide nanoparticles [6] that have been synthesized for various applications including medical and industrial uses, new compounds of symmetric crystals in the class of perovskites have found special applications. Consequently, perovskites exhibit a remarkable diversity of electronic and magnetic ground states, encompassing ferroelectricity in titanates (e.g., $BaTiO_3$) [7], high temperature superconductivity in cuprates [8], colossal magnetoresistance in manganites [9], and, more recently, outstanding photovoltaic performance in hybrid organic–inorganic halides [10,11].

The modern surge in perovskite research was catalyzed by the 2009 report by Kojima et al., who employed methylammonium lead iodide ($MAPbI_3$) as a sensitizer in a dye sensitized solar cell, achieving a power conversion efficiency (PCE) of 3.8% [12]. The subsequent introduction of solid state hole transporting layers by Kim et al. in 2012 marked a pivotal advance, elevating efficiencies to approximately 10% while dramatically improving device stability [13]. Since then, certified PCEs for single junction perovskite solar cells (PSCs) have surpassed 26%, positioning them as a credible competitor to established photovoltaic technologies [14]. Beyond photovoltaics, metal halide perovskites have demonstrated external quantum efficiencies (EQEs) exceeding 20% in Perovskite light-emitting diode (PeLEDs) [15], and have exhibited exceptional sensitivity as X ray and visible light detectors [16].

The objective of this short review is to provide a focused yet comprehensive account of perovskite materials science, with an emphasis on the structure property relationships that underpin their technological relevance. The discussion begins with the crystallographic foundations of the perovskite structure and the compositional diversity across oxide, halide, hybrid organic-inorganic, and double perovskite families. Recent discoveries that have expanded the compositional space are presented in a structured tabular format. Subsequently, the principal synthetic routes for preparing perovskite materials in various morphologies single crystals, thin films, and nanocrystals are summarized, accompanied by a second table detailing recent methodological advances. The central portion of the review critically examines the optoelectronic applications that have driven the field's rapid expansion, particularly in photovoltaics, light emission, and photodetection. The persistent challenge of long term stability is analyzed in depth, with a focus on degradation mechanisms and state of the art mitigation strategies. The review concludes with a perspective on future directions, including lead free alternatives, chiral hybrid perovskites, scalability, and integration with silicon photovoltaics.

2. Structural and Compositional Diversity

2.1 Crystallographic Principles

The ideal perovskite structure is cubic with space group $Pm\bar{3}m$, characterized by a primitive unit cell in which the B site cation occupies the octahedral interstices coordinated by six X anions, while the A site cation occupies the cuboctahedral cavity coordinated by twelve X anions [1]. In practice, deviations from ideality are ubiquitous, driven by geometric constraints that lead to tilting of the BX_6 octahedra and consequent symmetry lowering to tetragonal, orthorhombic, or rhombohedral phases. The stability and degree of distortion are quantitatively described by the Goldschmidt tolerance factor t and the octahedral factor μ [17].

$$t = \frac{(r_A + r_x)}{\sqrt{2}\,(r_B + r_x)}, \qquad \mu = \frac{r_B}{r_x}$$

The ionic radius rA corresponds to the A-site cation in 12-fold (cuboctahedral) coordination, with typical examples including Cs^+ and the effective radius of $CH_3NH_3^+$. The radius rB represents the B-site cation in 6-fold (octahedral) coordination, such as Pb^{2+}, Sn^{2+}, or Ti^{4+}. The radius rX refers to the X-site anion and is typically taken for 6-fold coordination to maintain consistency with the B–X bonding

in perovskite structures. Stable perovskites typically exhibit 0.8< t < 1.0, with μ exceeding a composition dependent threshold. When t deviates substantially from unity, cooperative octahedral tilting reduces the coordination number of the A site and often engenders ferroelectric or antiferrodistortive instabilities [17].

2.2 Compositional Classes

Perovskites are generally classified into three principal categories based on the nature of their constituent ions. Among these, oxide perovskites (e.g., $BaTiO_3$, $SrTiO_3$, $LaMnO_3$) represent the classical and most widely studied family. Synthesized at high temperatures, they exhibit robust mechanical and chemical stability. Their functional properties span ferroelectricity, piezoelectricity, high temperature superconductivity, and colossal magnetoresistance, forming the basis for applications in capacitors, actuators, solid oxide fuel cells, and spintronics [7-9,18].

Barium titanate ($BaTiO_3$) is a prototypical perovskite oxide that exhibits a well-defined sequence of temperature-driven structural phase transitions (Tp) under ambient conditions (Figure 1). At high temperatures, it adopts a centrosymmetric cubic phase, which transforms upon cooling into tetragonal, orthorhombic, and finally rhombohedral phases [19]. These four equilibrium crystal structures differ in symmetry and polarization behavior, with the cubic phase being paraelectric and the lower-symmetry phases exhibiting ferroelectricity due to the displacement of Ti ions. This progression provides a fundamental framework for understanding the structural, dielectric, and functional properties of perovskite materials.

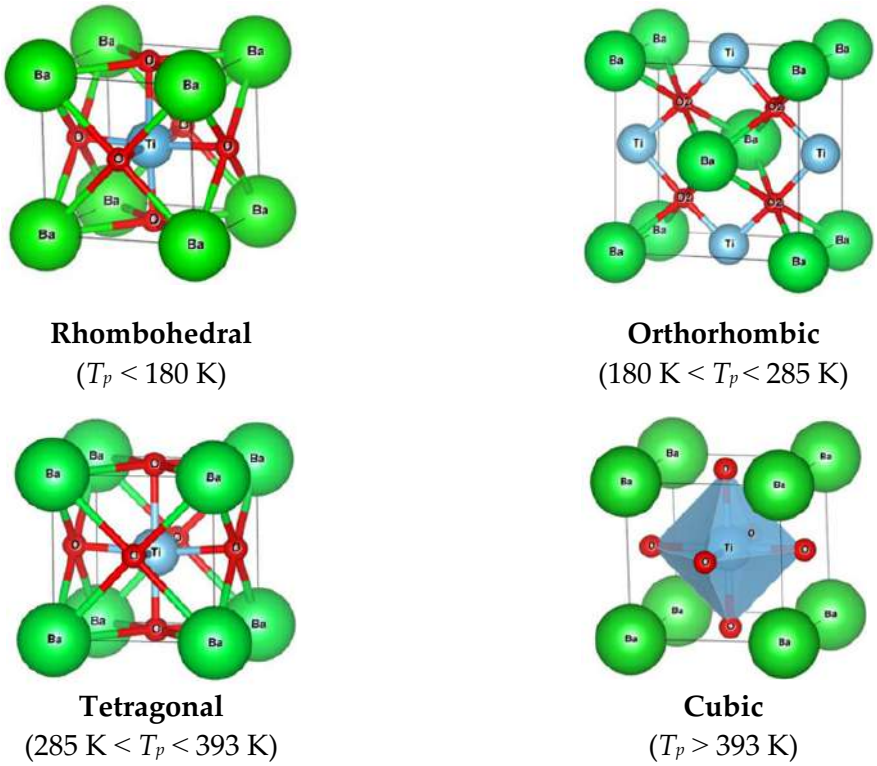

Figure 1. The various phases of $BaTiO_3$ as a perovskite oxide and the effect of temperature variations on its crystal structure [19].

Metal halide perovskites adopt the general ABX_3 stoichiometry, where X represents a halide anion (I^-, Br^-, Cl^-), B is a divalent metal cation (commonly Pb^{2+} or Sn^{2+}), and A is a monovalent cation that can be either inorganic (e.g., Cs^+) or organic (e.g., methylammonium (MA^+) and formamidinium (FA^+)). This class of materials has attracted considerable attention due to its outstanding optoelectronic properties, including high absorption coefficients (>10^4 cm^{-1}), long charge carrier

diffusion lengths (often exceeding several micrometers in single crystals), and a compositionally tunable bandgap spanning the visible spectrum (1.2–2.3 eV) [10,11]. Moreover, these materials exhibit notable defect tolerance, with relatively few deep trap states despite being processed via solution-based methods [20].

Hybrid (organic–inorganic) perovskites constitute a distinct subclass of metal halide perovskites in which the A-site is occupied by an organic cation, effectively bridging molecular and solid-state chemistry (Figure 2). Representative examples include MA^+- and FA^+-based compounds such as $MAPbI_3$ and $FAPbI_3$ [21]. As illustrated in Figure 2a, the crystal structure consists of an organic A-site cation (e.g., $CH_3NH_3^+$), a metal B-site cation (Pb^{2+}), and a halide X-site anion (I^-). These components form a three-dimensional framework through interactions between the organic cation and the inorganic lattice. The A-site composition can be further extended to include chiral organic cations, enabling the formation of chiral hybrid perovskites with unique chiroptical functionalities [22-24]. The corresponding unit cell, shown in Figure 2b, adopts a cubic structure. This hybrid architecture results in structural softness, which contributes to excellent optoelectronic performance while also enabling low-temperature solution processing, a key advantage over oxide perovskites [25,26].

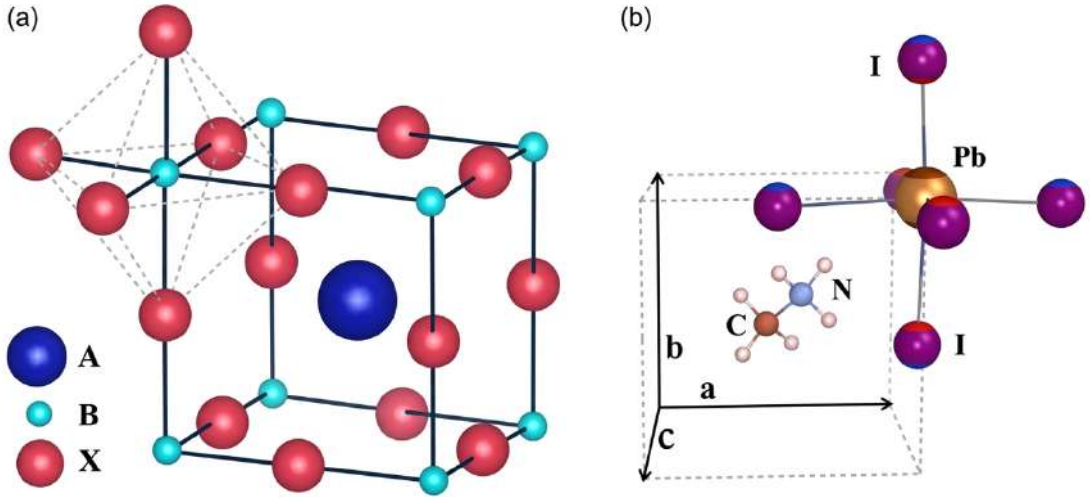

Figure 2. a) Crystal structure of the widely used halide perovskite $CH_3NH_3PbI_3$, in which the A-site is occupied by an organic cation ($CH_3NH_3^+$), the B-site by a metal cation (Pb^{2+}), and the X-site by a halide anion (I^-). b) Unit cell of $CH_3NH_3PbI_3$ exhibiting a cubic crystal structure.

The term perovskite refers to any compound which has an ABX3 crystal structure, where A and B are two different cations and X is the anion. The highest performing and most widely studied perovskite for photovoltaic applications is methylammonium lead iodide (CH3NH3PbI3), also known as MAPI, the structure of which is shown in Figure 3. The lead cation (blue) is located in the centre of a cube of methylammonium cations (green) and is surrounded by an octahedron of iodide anions (red). There are three different phases of the crystal structure that MAPI can adopt, with the temperature controlling which phase is thermodynamically stable. At room temperature MAPI is known to be in the tetragonal phase where two of the unit cell lengths are equivalent ($a = b \neq c$). At lower temperatures the tetragonal symmetry is broken and MAPI adopts the orthorhombic structure where all three-unit cell lengths are different ($a \neq b \neq c$) [27]. At elevated temperatures the symmetry of the structure increases, with MAPI adopting the cubic crystal structure ($a = b = c$). The temperature of the transitions between these three structures can be determined using photoluminescence spectroscopy.

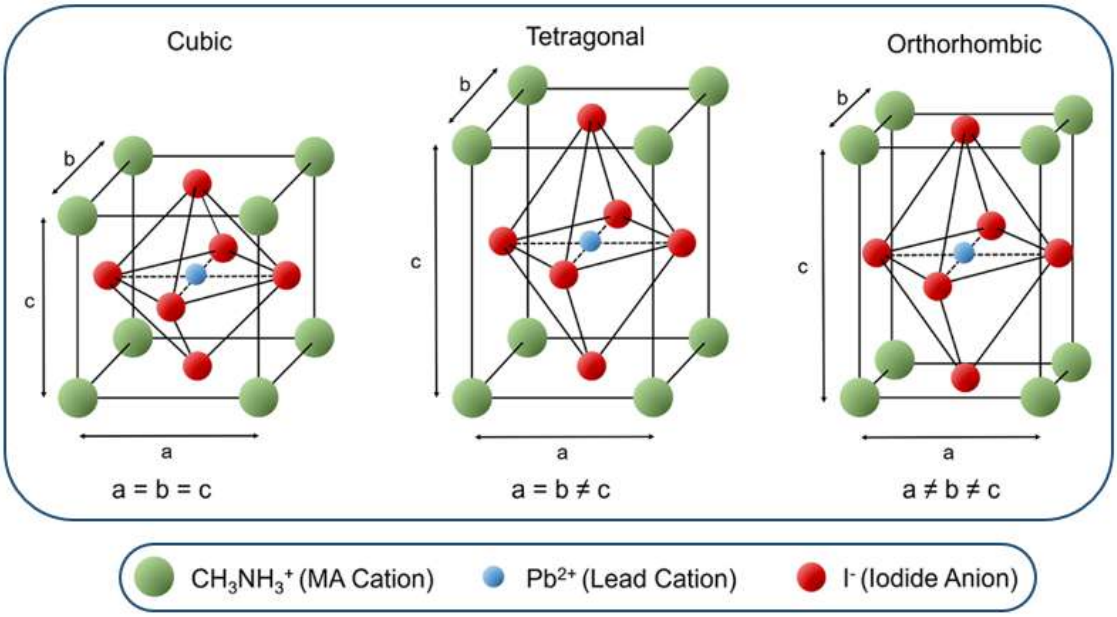

Figure 3. Crystal unit cells corresponding to the cubic, tetragonal, and orthorhombic phases of MAPI perovskite [27].

Double perovskites ($A_2BB'X_6$) have emerged as a promising strategy to mitigate the toxicity associated with lead-based perovskites. In these structures, two Pb^{2+} ions are replaced by a combination of a monovalent and a trivalent metal cation (e.g., Ag^{+} and Bi^{3+}), thereby preserving overall charge neutrality. A representative example is cesium silver bismuth bromide ($Cs_2AgBiBr_6$), whose crystal structure is illustrated in Figure 4. This material exhibits enhanced ambient stability and reduced toxicity compared to lead-based counterparts; however, its optical properties currently result in lower photovoltaic performance than conventional lead halide perovskites [28].

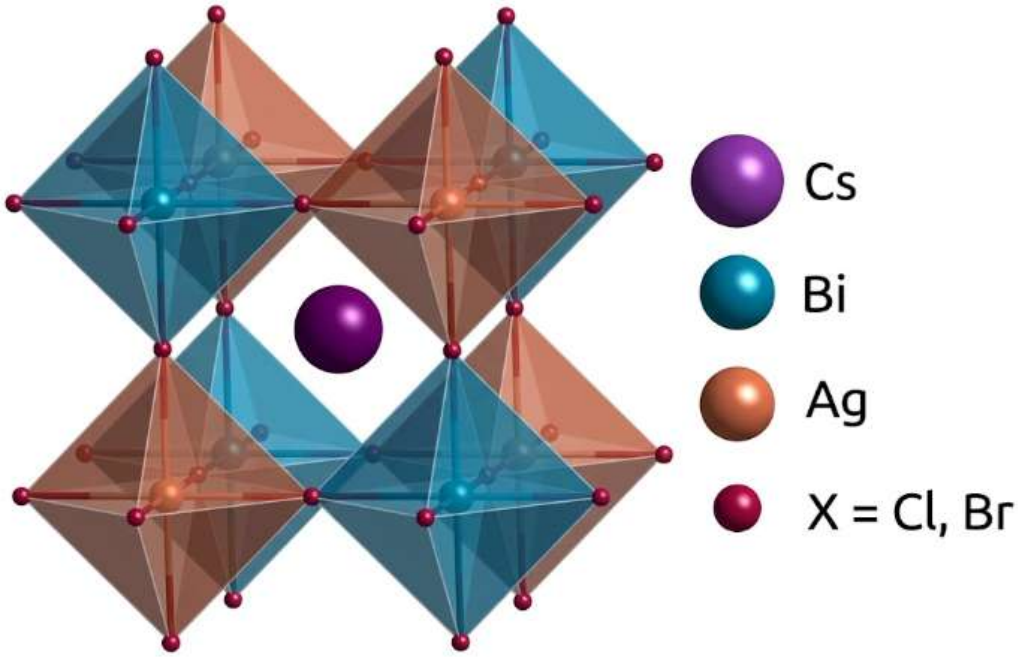

Figure 4. A ball-and-stick schematic illustration of the double perovskite crystal structure. Large purple spheres represent A-site Cesium (Cs) cations. The structure features alternating corner-sharing octahedral frameworks: teal spheres (B-site Bi^{3+}) form teal polyhedra, and orange-copper spheres (B'-site Ag^{+}) form brown-copper polyhedra. Small red spheres at the octahedral corners correspond to halide anions (X = Cl, Br). The key highlights the specific colors used for each atomic species.

However, this hybrid nature also introduces challenges, including susceptibility to moisture and thermal degradation, driving current research toward compositional engineering and dimensionality reduction to enhance stability without sacrificing performance for photovoltaic and light-emitting applications [29]. Recent investigations have considerably expanded the compositional landscape, revealing novel compounds and unexpected functionalities. Table 1 summarizes selected recent findings that exemplify the ongoing diversification of perovskite materials across structural dimensions, chemical compositions, and application domains.

The entries in Table 1 illustrate that contemporary perovskite research extends far beyond the canonical three-dimensional metal halides, encompassing low-dimensional architectures, lead-free compositions, oxide functional materials, and heterointerface phenomena. This structural and compositional richness continues to fuel discoveries across optoelectronics, spintronics, and quantum information science.

3. Synthesis Methods

The functional properties of perovskite materials are intimately linked to their crystalline quality, morphology, and defect landscape, all of which are governed by the synthesis route. Different applications demand distinct form factors, ranging from bulk single crystals for fundamental characterization to large-area thin films for devices and colloidal nanocrystals for luminescent applications. Recent years have witnessed substantial methodological innovations aimed at enhancing reproducibility, scalability, and material quality. Table 2 summarizes selected recent advances in perovskite synthesis across different material classes and morphologies.

The methods summarized in Table 2 reflect the ongoing maturation of perovskite synthesis from laboratory-scale spin-coating toward industrially relevant techniques. Solution-based methods, including ITC [50], antisolvent engineering [51], and slot-die coating [58], remain dominant due to their low cost and versatility. Vapor-phase techniques such as sequential vapor deposition [54], and CVD [57], offer superior thickness control, conformality, and compatibility with multilayer architectures, making them attractive for tandem solar cells and complex device stacks. Colloidal synthesis routes, particularly hot-injection [53], and LARP [55], have enabled the production of nanocrystals with near-unity photoluminescence quantum yields, driving advances in display technology. Scalable deposition methods, exemplified by slot-die coating with gas quenching [58], have demonstrated that high efficiencies can be maintained on large-area modules, addressing a critical prerequisite for commercial translation.

Table 1. Recent research findings across perovskite material classes.

Composition	Class	Key Finding	Property/Performance	Application	Ref.
$Cs_{0.05}FA_{0.85}MA_{0.10}Pb(I_{0.95}Br_{0.05})_3$	Metal halide (triple-cation)	Incorporation of a 2D perovskite layer at the interface reduces non-radiative recombination and improves stability	Certified PCE = 25.2%	Solar cells	[30]
Cesium lead iodide ($CsPbI_3$) quantum dots	Metal halide (inorganic)	Short-chain zwitterionic ligands enhance charge transport while maintaining colloidal stability	PCE = 15.1%; operational stability > 1000 h	Photovoltaics	[31]
$Cs_2AgBiBr_6$	Double halide	High defect tolerance arises from a flat valence band maximum; carrier lifetimes exceed 100 ns	PCE = 3.2% in planar devices	Lead-free photovoltaics	[32]
$(PEA)_2(MA)_{n-1}Pb_nBr_{3n+1}$ (n = 3)	2D Ruddlesden–Popper	Dielectric confinement enhances exciton binding energy, leading to near-unity photoluminescence quantum yield	EQE = 22.5% in green PeLEDs	Light-emitting diodes	[33]
$FASnI_3$ with SnF_2 and hydrazine	Lead-free halide	Reduction of Sn^{4+} content via hydrazine vapor treatment suppresses p-type self-doping	PCE = 14.6%; improved reproducibility	Lead-free solar cells	[34]
$BaTiO_3$	Oxide (ferroelectric)	Engineered domain wall conductivity via epitaxial strain enables resistive switching with high on/off ratio	Conductivity modulation > 10^4	Neuromorphic computing	[35]
$La_{0.7}Sr_{0.3}MnO_3$	Oxide (manganite)	Interfacial symmetry mismatch with $SrTiO_3$ induces perpendicular magnetic anisotropy at room temperature	Magnetic anisotropy energy ~ 10^5 J m^{-3}	Spintronics	[36]
Cesium lead bromide ($CsPbBr_3$) nanocrystals	Metal halide (nanocrystal)	Reversible orthorhombic-to-tetragonal phase transition enables optical memory with high contrast	Photoluminescence switching contrast > 10^3	Optical data storage	[37]
Lanthanum aluminate ($LaAlO_3$)/$KTaO_3$	Oxide (heterointerface)	Superconductivity emerges at the (111) interface without polar discontinuity	*Tc* up to 2.0 K	Quantum electronics	[38]
$(MA)_3Bi_2I_9$	Lead-free halide (defect perovskite)	Zero-dimensional structure with strong quantum confinement yields high radioluminescence intensity	Light yield ~ 40,000 photons MeV^{-1}; detection limit < 10 nGy s^{-1}	X-ray scintillators	[39]

$CsPbI_3$ nanowires	Metal halide (1D)	Controlled orientation yields linearly polarized emission with anisotropy factor > 0.8	Polarized electroluminescence efficiency 12%	Polarized light sources	[40]
Strontium hafnate ($SrHfO_3$)	Oxide (high-κ dielectric)	Atomic layer deposition produces films with dielectric constant > 20 and breakdown field > 5 MV cm^{-1}	Equivalent oxide thickness < 0.8 nm	2D transistor gate dielectrics	[41]
$(FAPbI_3)_{0.95}(MAPbBr_3)_{0.05}$ with guanidinium doping	Hybrid (mixed-cation)	Guanidinium incorporation reduces lattice strain and suppresses non-radiative recombination, enabling high open-circuit voltage	PCE = 24.3% in inverted solar cells; VOC = 1.19 V	Photovoltaics	[42]
(R-/S-1-(1-naphthyl)ethylammonium)$_2PbI_4$	Chiral 2D hybrid	Strong chiroptical activity with circular dichroism dissymmetry factors up to 10–2; spin-selective charge transport	Circularly polarized light (CPL) detection with responsivity > 100 mA W–1	Chiral optoelectronics	[43]
$(PEA)_2MA_4Pb_5I1_6$ (n = 5)	2D Ruddlesden-Popper hybrid	Phase distribution engineering enhances charge transport while retaining moisture resistance; unencapsulated devices retain 90% efficiency after 1000 h	PCE = 18.8% in solar cells	Stable photovoltaics	[44]
(R-/S-MBA)$_2PbI_4$ (MBA = α-methylbenzylammonium)	Chiral 2D hybrid	Intrinsic chirality induces strong circularly polarized electroluminescence; dissymmetry factor gEL ≈ 0.3	EQE = 4.2% in circularly polarized OLEDs	Chiral light-emitting diodes	[45]
$(FA)_2CuxAg1{-}xBiI_6$	Hybrid double perovskite (lead-free)	Copper alloying lifts parity-forbidden transitions, improving absorption coefficient and carrier lifetime	PCE = 4.5% in air-processed solar cells; T80 > 2000 h	Lead-free photovoltaics	[46]
(N-methyl-2-pyrrolidone)$_2[Pb_2Br_6]$	0D hybrid (molecular)	Isolated metal halide octahedra give broadband white emission with high color rendering index; near-unity photoluminescence quantum yield	PLQY = 92%; stable over 6 months under ambient	Single-source white lighting	[47]
(R-/S-3-aminopiperidinium)$_2PbBr_4$	Chiral 2D hybrid	Ferroelastic domain switching coupled with circular dichroism; optically controllable polarization	Second-harmonic generation intensity 3× that of quartz	Chiral ferroelectrics & nonlinear optics	[48]

Table 2. Recent research findings on perovskite synthesis methods.

Method	Material System	Key Finding	Morphology	Application Focus	Ref
Inverse temperature crystallization (ITC)	$MAPbI_3$	Controlled supersaturation through temperature gradients yields crystals with reduced defect density (trap density ~ 2×10^9 cm^{-3})	Single crystals (centimeter scale)	Fundamental transport studies	[49]
Antisolvent-assisted spin coating	Triple-cation $Cs_{0.05}FA_{0.85}MA_{0.10}Pb(I_{0.95}Br_{0.05})_3$	Use of methyl acetate as antisolvent induces rapid nucleation, yielding pinhole-free films with grain sizes > 1 μm	Polycrystalline thin films	High-efficiency solar cells	[50]
Vapor-assisted solution processing (VASP)	$MAPbI_3$	Exposure of PbI_2 films to MAI vapor enables conformal conversion on textured substrates; eliminates antisolvent step	Thin films (large area)	Scalable photovoltaics	[51]
Hot-injection colloidal synthesis	$CsPbBr_3$ nanocrystals	Precise control of reaction temperature (150–180 °C) and ligand ratios yields monodisperse nanocrystals with Photoluminescence quantum yield (PLQY) > 95%	Nanocrystals (10–15 nm)	Displays and LEDs	[52]
Sequential vapor deposition	Formamidinium lead iodide ($FAPbI_3$)	Co-evaporation of PbI_2 and FAI followed by controlled annealing yields phase-pure α-$FAPbI_3$ with high crystallinity	Thin films (wafer-scale)	Tandem solar cells	[53]
Ligand-assisted reprecipitation (LARP)	$CsPbX_3$ (X = Cl, Br, I)	Room-temperature synthesis using polar solvents and antisolvent precipitation yields nanocrystals with tunable composition and bandgap	Nanocrystals (5–20 nm)	Lighting and lasing	[54]
Melt growth (Bridgman method)	$BaTiO_3$	Use of continuous feeding compensates for segregation, producing large-area single crystals with uniform composition	Single crystals (wafer-scale)	Piezoelectric actuators	[55]
Chemical vapor deposition (CVD)	$CsPbBr_3$	Two-zone CVD with separate CsPbX and $PbBr_2$ precursors yields high-quality nanowires with controlled orientation	Nanowires (diameter 50–200 nm)	Photodetectors	[56]
Slot-die coating	$FA_{0.85}Cs_{0.15}PbI_3$	Blade coating with gas quenching enables high-throughput deposition; PCE of 21.5% on 100 cm^2 modules	Thin films (large-area modules)	Industrial scaling	[57]
Seeded growth (solution)	$FAPbI_3$	Pre-synthesized $FAPbI_3$ seeds enable uniform crystallization and suppress δ-phase formation.	Polycrystalline thin films	Stable solar cells	[58]

4. Optoelectronic Applications

4.1 Perovskite Solar Cells

The development of perovskite solar cells (PSCs) represents one of the most rapid ascents in photovoltaic history. Following the initial demonstrations, the field has achieved certified single-junction PCEs exceeding 26% [14]. This progress has been driven by iterative refinements in composition and interface engineering. Triple-cation compositions (Cs/FA/MA) have emerged as a benchmark due to their superior thermal stability and high efficiency [59]. The incorporation of two-dimensional perovskite layers at the top and bottom interfaces effectively passivates surface defects and suppresses non-radiative recombination, enabling open-circuit voltages approaching the Shockley–Queisser limit [31].

A particularly promising pathway to commercialization is the integration of perovskites into tandem solar cells. By combining a wide-bandgap perovskite top cell (optimized for blue and green absorption) with a silicon bottom cell, efficiencies exceeding 33% have been demonstrated in monolithic two-terminal tandems [60]. Such architectures surpass the theoretical efficiency limit of single-junction silicon while leveraging the established silicon manufacturing infrastructure.

4.2 Perovskite Light-Emitting Diodes

Whereas solar cells exploit efficient charge generation, light-emitting diodes (LEDs) require efficient radiative recombination of injected carriers. In three-dimensional metal halide perovskites, the relatively low exciton binding energy (typically < 50 meV) results in a high fraction of free carriers that are susceptible to non-radiative recombination at defects [61]. The breakthrough for PeLEDs came with the introduction of low-dimensional structures nanocrystals, quantum wells, and 2D Ruddlesden–Popper phases that enhance exciton confinement and radiative efficiency [62,63]. Green and red PeLEDs now routinely achieve EQEs exceeding 20%, rivaling the best organic LEDs. Blue emission remains more challenging due to halide phase segregation and ion migration under electrical bias; however, strategies such as compositional grading and the use of quasi-2D structures have yielded steady improvements [64]. The exceptionally narrow emission linewidths (< 20 nm) of perovskite emitters position them strongly for next-generation ultra-high-definition displays.

The development of circularly polarized light-emitting diodes based on chiral hybrid organic-inorganic perovskites is of particular interest [65]. By incorporating chiral organic cations or chiral surface ligands, the resulting materials exhibit chiroptical activity, enabling direct generation of circularly polarized luminescence without external optical components [66]. Anisotropy factors glum approaching 10^{-2} have been demonstrated in chiral 2D perovskites, though further improvements are needed to rival the performance of achiral PeLEDs [22,67]. This capability is highly attractive for applications in 3D displays, optical communication, and quantum information technologies.

4.3 Photodetectors and Radiation Detectors

The combination of high X-ray attenuation coefficients (owing to the presence of high-atomic-number elements such as Pb and I) and outstanding charge-transport properties (mobility–lifetime products exceeding 10^{-3} cm^2 V^{-1}) makes metal halide perovskites highly effective

for ionizing radiation detection [16]. Solution-processed polycrystalline thick films and single crystals have demonstrated sensitivities to X-rays exceeding 10^4 μC Gy^{-1} cm^{-2}, surpassing amorphous selenium (a-Se), the current clinical standard [44]. In the visible range, perovskite photodetectors exhibit high responsivity (>1 A W^{-1}) and fast response times (<1 μs), rendering them suitable for optical communication and imaging systems [68,69].

Beyond conventional photodetection, chiral hybrid perovskites have emerged as promising materials for the direct detection of CPL due to their intrinsic chirality and outstanding optoelectronic properties [70]. Devices based on chiral organic–inorganic hybrid perovskites demonstrate high responsivity and stability without the need for external optical elements, enabling integrated CPL photodetectors [71]. Advances include one dimensional helical perovskite structures achieving polarization discrimination ratios up to 25.4, surpassing traditional chiral plasmonic metamaterials [72], and the incorporation of ferroelectricity and Rashba effects further enhances CPL detection through switchable self-powered operation.

5. Stability Challenges and Mitigation Strategies

Despite their exceptional performance, metal halide perovskites are intrinsically susceptible to degradation under environmental stressors. Moisture induces hydration and subsequent decomposition to PbX_2 and AX [73]. Oxygen, particularly under illumination, can generate superoxide radicals that oxidize the organic cations and disrupt the lattice [74]. Elevated temperatures cause volatilization of organic components and, in the case of $FAPbI_3$, a phase transition from the photoactive black α-phase to the non-perovskite yellow δ-phase [75]. Under operational conditions, ion migration and, in mixed-halide systems, photo-induced phase segregation further degrade device performance [76].

Three principal mitigation strategies have emerged. Compositional engineering replaces volatile MA^+ with a mixture of FA^+ and Cs^+, yielding thermally robust absorbers [60]. The incorporation of large organic cations to form 2D perovskites at grain boundaries or surfaces dramatically enhances moisture resistance, though care must be taken to avoid impeding charge transport [77]. Interfacial passivation involves the deposition of thin layers of hydrophobic polymers, metal oxides (e.g., Al_2O_3), or 2D materials (e.g., graphene) that block moisture ingress and heal surface defects [78]. Encapsulation using glass or multi-layer barrier films isolates the device from ambient atmosphere; with optimized encapsulation, operational lifetimes exceeding 10,000 hours under continuous illumination have been reported [79].

6. Future Perspectives

The maturation of perovskite research has brought the field to the threshold of commercial relevance. However, several critical challenges must be addressed to enable large-scale deployment. Lead toxicity remains a pressing concern. While encapsulation can effectively contain lead within a device, environmental and regulatory pressures are driving the search for lead-free alternatives. Tin-based perovskites such as Formamidinium tin iodide (e.g., $FASnI_3$) have achieved PCEs approaching 15% [35], while double perovskites such as $Cs_2AgBiBr_6$ offer enhanced stability [33]. Realizing performance parity with lead-based systems will require deeper understanding of defect chemistry and advanced doping strategies. Scalable manufacturing is another critical hurdle. Spin-coating, while effective for laboratory cells, is not amenable to large-area production. Scalable methods such as slot-die coating, spray coating, and vapor deposition must be refined to deliver

uniform, high-quality films over square-meter areas [58]. Concurrently, the development of robust, low-cost encapsulation technologies that meet the stringent lifetime requirements of outdoor photovoltaics (25–30 years) is essential.

Beyond established material families, chiral hybrid perovskites are emerging as a platform for integrating optoelectronic functionality with spin- and chirality-dependent phenomena. The transfer of molecular chirality to the inorganic framework enables CPL emission, spin-selective charge transport, and nonlinear optical activity [80]. While still in an early stage, these materials hold promise for next-generation displays, spintronic devices, and quantum light sources, provided that challenges in achieving high anisotropy factors alongside high device efficiencies can be addressed [81]. The recently observed nonlinear relation between anisotropy factors and enantiomeric excess in chiral perovskites, provides a new avenue for tunability [82]. Varying the enantiomeric excess has recently emerged as a powerful approach to nonlinearly enhance chiroptical response, providing a new degree of tunability for chiral perovskites .[83,84]

In the near term, tandem integration with silicon represents the most commercially viable path for perovskite photovoltaics. Research efforts are increasingly focused on developing stable interconnection layers, optimizing transparent electrodes, and ensuring the long-term operational stability of the perovskite top cell under real-world conditions [61]. Simultaneously, the exceptional luminescent properties of perovskite nanocrystals are being actively explored by the display industry, with prototype PeLED displays demonstrating superior color gamut and efficiency [53].

7. Conclusion

In conclusion, perovskite materials have evolved from a mineralogical curiosity to a cornerstone of modern materials science. The remarkable optoelectronic properties of metal halide perovskites, combined with the structural versatility of the broader perovskite family, have enabled unprecedented advances in photovoltaics, light emission, and photo-detection. The distinct characteristics of hybrid organic–inorganic perovskites have been central to these advances, while chiral hybrid perovskites are opening new frontiers in spin- and light-controlled devices. Although challenges related to stability, lead toxicity, and scalability persist, the convergence of fundamental understanding, engineering innovation, and industrial investment suggests that perovskites will play a transformative role in next-generation electronic and energy technologies. Continued exploration of both oxide and halide systems promises not only to overcome existing limitations but also to uncover new phenomena and applications yet to be conceived.

Acknowledgement

During the preparation of this manuscript, the authors used ChatGPT-5 to assist in organizing and integrating the discussed topics into a coherent narrative. The authors have reviewed and edited the generated content and take full responsibility for the final version of the publication.

References

1. Katz, E.A. Perovskite: name puzzle and German-Russian odyssey of discovery. *Helvetica Chimica Acta* **2020**, *103*, e2000061.
2. Jazayeri, S.D.; Ideris, A.; Zakaria, Z.; Shameli, K.; Moeini, H.; Omar, A.R. Cytotoxicity and immunological responses following oral vaccination of nanoencapsulated avian influenza

virus H5 DNA vaccine with green synthesis silver nanoparticles. *Journal of Controlled Release* **2012**, *161*, 116-123, doi:https://doi.org/10.1016/j.jconrel.2012.04.015.

3. Lee, K.X.; Shameli, K.; Mohamad, S.E.; Yew, Y.P.; Mohamed Isa, E.D.; Yap, H.-Y.; Lim, W.L.; Teow, S.-Y. Bio-Mediated Synthesis and Characterisation of Silver Nanocarrier, and Its Potent Anticancer Action. *Nanomaterials* **2019**, *9*, 1423.
4. Shameli, K.; Ahmad, M.B.; Al-Mulla, E.A.J.; Shabanzadeh, P.; Bagheri, S. Antibacterial effect of silver nanoparticles on talc composites. *Research on Chemical Intermediates* **2015**, *41*, 251-263, doi:10.1007/s11164-013-1188-y.
5. Lee, K.X.; Shameli, K.; Miyake, M.; Khairudin, N.B.B.A.; Mohamad, S.E.B.; Hara, H.; Nordin, M.F.B.M.; Yew, Y.P. Gold Nanoparticles Biosynthesis: A Simple Route for Control Size Using Waste Peel Extract. *IEEE Transactions on Nanotechnology* **2017**, *16*, 954-957, doi:10.1109/TNANO.2017.2728600.
6. Teow, S.-Y.; Wong, M.M.-T.; Yap, H.-Y.; Peh, S.-C.; Shameli, K. Bactericidal Properties of Plants-Derived Metal and Metal Oxide Nanoparticles (NPs). *Molecules* **2018**, *23*, 1366.
7. Okumura, R.; Oku, T.; Suzuki, A. Electronic structures of ABX3 perovskite crystals with a monovalent copper ion as the A-site cation. *Chemical Physics Impact* **2024**, *8*, 100534.
8. Huang, Z.; Liu, G.; Fu, Y.; Yan, M. First-Principles Insight on Electronic and Magnetic Properties of SrFeTe-Based Double and Triple Perovskites. *Inorganic Chemistry* **2025**, *64*, 14261-14271.
9. Boora, N.; Ahmad, R.; Rahman, S.; Dung, N.Q.; Ahmad, A.; Alshammari, M.B.; Lee, B.-I. Recent advances of colossal magnetoresistance in versatile La-Ca-Mn-O material-based films. *Magnetochemistry* **2025**, *11*, 5.
10. Montecucco, R.; Quadrivi, E.; Po, R.; Grancini, G. All-inorganic cesium-based hybrid perovskites for efficient and stable solar cells and modules. *Advanced Energy Materials* **2021**, *11*, 2100672.
11. Krishnamurthy, S.; Pandey, P.; Kaur, J.; Chakraborty, S.; Nayak, P.K.; Sadhanala, A.; Ogale, S. Organic–inorganic hybrid and inorganic halide perovskites: structural and chemical engineering, interfaces and optoelectronic properties. *Journal of Physics D: Applied Physics* **2021**, *54*, 133002.
12. Ahmad, Z.; Scheidt, R.A.; Hautzinger, M.P.; Zhu, K.; Beard, M.C.; Galli, G. Understanding the effect of lead iodide excess on the performance of methylammonium lead iodide perovskite solar cells. *ACS Energy Letters* **2022**, *7*, 1912-1919.
13. Li, S.; Cao, Y.-L.; Li, W.-H.; Bo, Z.-S. A brief review of hole transporting materials commonly used in perovskite solar cells. *Rare Metals* **2021**, *40*, 2712-2729.
14. Yang, C.; Hu, W.; Liu, J.; Han, C.; Gao, Q.; Mei, A.; Zhou, Y.; Guo, F.; Han, H. Achievements, challenges, and future prospects for industrialization of perovskite solar cells. *Light: Science & Applications* **2024**, *13*, 227.
15. Liu, X.-K.; Xu, W.; Bai, S.; Jin, Y.; Wang, J.; Friend, R.H.; Gao, F. Metal halide perovskites for light-emitting diodes. *Nature Materials* **2021**, *20*, 10-21.
16. Wu, H.; Ge, Y.; Niu, G.; Tang, J. Metal halide perovskites for X-ray detection and imaging. *Matter* **2021**, *4*, 144-163.

17. Fedorovskiy, A.E.; Drigo, N.A.; Nazeeruddin, M.K. The role of Goldschmidt's tolerance factor in the formation of A2BX6 double halide perovskites and its optimal range. *Small Methods* **2020**, *4*, 1900426.
18. Irvine, J.; Rupp, J.L.; Liu, G.; Xu, X.; Haile, S.; Qian, X.; Snyder, A.; Freer, R.; Ekren, D.; Skinner, S. Roadmap on inorganic perovskites for energy applications. *Journal of Physics: Energy* **2021**, *3*, 031502.
19. Aithal, G.S.; M, P.; Pandey, S.; Trivedi, R.; Kamath, S.D.; Negi, D.; Mishra, V. First principles study of defect-induced electronic properties across temperature-dependent phases of $BaTiO_3$. *Chemical Physics* **2026**, *607*, 113150, doi:https://doi.org/10.1016/j.chemphys.2026.113150.
20. Bao, C.; Gao, F. Physics of defects in metal halide perovskites. *Reports on Progress in Physics* **2022**, *85*, 096501.
21. Lee, J.H.; Lee, J.-H.; Kong, E.-H.; Jang, H.M. The nature of hydrogen-bonding interaction in the prototypic hybrid halide perovskite, tetragonal $CH_3NH_3PbI_3$. *Scientific Reports* **2016**, *6*, 21687, doi:10.1038/srep21687.
22. Liu, S.; Kepenekian, M.; Bodnar, S.; Feldmann, S.; Heindl, M.W.; Fehn, N.; Zerhoch, J.; Shcherbakov, A.; Pöthig, A.; Li, Y.; et al. Bright circularly polarized photoluminescence in chiral layered hybrid lead-halide perovskites. *Sci Adv* **2023**, *9*, eadh5083, doi:10.1126/sciadv.adh5083.
23. Liu, S.; Heindl, M.W.; Fehn, N.; Caicedo-Dávila, S.; Eyre, L.; Kronawitter, S.M.; Zerhoch, J.; Bodnar, S.; Shcherbakov, A.; Stadlbauer, A.; et al. Optically Induced Long-Lived Chirality Memory in the Color-Tunable Chiral Lead-Free Semiconductor (R)/(S)-$CHEA_4Bi_2BrxI10_{-x}$ (x = 0–10). *Journal of the American Chemical Society* **2022**, *144*, 14079-14089, doi:10.1021/jacs.2c01994.
24. Heindl, M.W.; Kodalle, T.; Fehn, N.; Reb, L.K.; Liu, S.; Harder, C.; Abdelsamie, M.; Eyre, L.; Sharp, I.D.; Roth, S.V.; et al. Strong Induced Circular Dichroism in a Hybrid Lead-Halide Semiconductor Using Chiral Amino Acids for Crystallite Surface Functionalization. *Advanced Optical Materials* **2022**, *10*, 2200204, doi:https://doi.org/10.1002/adom.202200204.
25. Jiang, J.; Vicent-Luna, J.M.; Tao, S. The role of solvents in the formation of methylammonium lead triiodide perovskite. *Journal of Energy Chemistry* **2022**, *68*, 393-400, doi:https://doi.org/10.1016/j.jechem.2021.12.030.
26. Ferreira, A.C.; Létoublon, A.; Paofai, S.; Raymond, S.; Ecolivet, C.; Rufflé, B.; Cordier, S.; Katan, C.; Saidaminov, M.I.; Zhumekenov, A.A.; et al. Elastic Softness of Hybrid Lead Halide Perovskites. *Physical Review Letters* **2018**, *121*, 085502, doi:10.1103/PhysRevLett.121.085502.
27. Mavuso, M.A.; Msimanga, M. Mitigating Environmental Effects in Halide Perovskites through Hybrid Perovskite-Polymer Nanocomposites: A Short Review. *Photonics* **2023**, *10*, 1242.
28. Tailor, N.K.; Listorti, A.; Colella, S.; Satapathi, S. Lead-free halide double perovskites: fundamentals, challenges, and photovoltaics applications. *Advanced Materials Technologies* **2023**, *8*, 2200442.

29. Maziviero, F.V.; Melo, D.M.A.; Medeiros, R.L.B.A.; Oliveira, Â.A.S.; Macedo, H.P.; Braga, R.M.; Morgado, E. Advancements and Prospects in Perovskite Solar Cells: From Hybrid to All-Inorganic Materials. *Nanomaterials* **2024**, *14*, 332.
30. Malouangou, M.D.; Zhang, Y.; Yang, Y.; Mbumba, M.T.; Akram, M.W.; Rop, E.; Matondo, J.T.; Guli, M. Enhancing the efficiency and stability of 2D-3D perovskite solar cells with embedded interface passivation with diammonium cation spacer. *Solar Energy Materials and Solar Cells* **2023**, *251*, 112135.
31. Gamal, A.; Alruqi, M.; Rabia, M. CsPbI3 lead and CsSnI3 lead-free perovskite materials for solar cell device. *International Journal of Energy Research* **2022**, *46*, 21739-21756.
32. Ullah, S.; Alshahrani, T.; Khan, F. Investigating the potential of lead-free Cs_2AgBiI_6 and $Cs_2AgBiBr_6$ double perovskites for photovoltaic applications. *Materials Today Communications* **2024**, *38*, 108514.
33. Tan, J.; Jiang, X.; Liu, D.; Tang, Z.-K.; Chulkov, E.V.; Vasenko, A.S. Exciton properties and broadband emission in two-dimensional Ruddlesden–Popper perovskites. *The Journal of Physical Chemistry Letters* **2025**, *16*, 7659-7665.
34. Bhuvaneswari, P.; Sriramalakshmi, P. Lead-Free pn Homojunction Cs-Doped and Pure $FASnI_3$-based perovskite solar cells–a performance analysis using SCAPS 1D simulator. *Results in Engineering* **2025**, *26*, 104779.
35. Jiang, Y.-F.; Peng, H.-Y.; Cai, Y.; Xu, Y.-T.; Fu, M.-Y.; Feng, M.; Wang, B.-W.; Wang, Y.-Q.; Guan, Z.; Chen, B.-B. Adaptive ferroelectric memristors with high-throughput $BaTiO_3$ thin films for neuromorphic computing. *Materials Horizons* **2025**, *12*, 6928-6937.
36. Chaluvadi, S.K.; Ajejas, F.; Orgiani, P.; Rousseau, O.; Vinai, G.; Petrov, A.Y.; Torelli, P.; Pautrat, A.; Camarero, J.; Perna, P. Room temperature biaxial magnetic anisotropy in La0. 67Sr0. 33MnO3 thin films on $SrTiO_3$ buffered MgO (001) substrates for spintronic applications. *Applied Physics Letters* **2018**, *113*.
37. Li, M.-X.; Huang, J.-Z.; Song, K.-Z.; Yao, W.-Y.; Jiang, F.-L. Stable Blue $CsPbBr_3$ Perovskite Nanocrystals with Near-Unity Photoluminescence Quantum Yield by Surface Ligand Engineering. *ACS Applied Materials & Interfaces* **2025**, *17*, 25702-25712.
38. Chen, Z.; Liu, Z.; Sun, Y.; Chen, X.; Liu, Y.; Zhang, H.; Li, H.; Zhang, M.; Hong, S.; Ren, T. Two-dimensional superconductivity at the $LaAlO_3/KTaO_3$ (110) heterointerface. *Physical Review Letters* **2021**, *126*, 026802.
39. Liu, Y.; Zhang, Y.; Yang, Z.; Cui, J.; Wu, H.; Ren, X.; Zhao, K.; Feng, J.; Tang, J.; Xu, Z. Large lead-free perovskite single crystal for high-performance coplanar X-ray imaging applications. *Advanced Optical Materials* **2020**, *8*, 2000814.
40. Gao, Y.; Zhao, L.; Shang, Q.; Zhong, Y.; Liu, Z.; Chen, J.; Zhang, Z.; Shi, J.; Du, W.; Zhang, Y. Ultrathin $CsPbX_3$ nanowire arrays with strong emission anisotropy. *Advanced Materials* **2018**, *30*, 1801805.
41. Kim, J.; Song, D.; Yun, H.; Lee, J.; Kim, J.H.; Kim, J.H.; Kim, B.; Char, K. Low leakage in high-k perovskite gate oxide $SrHfO_3$. *Advanced Electronic Materials* **2023**, *9*, 2201341.
42. De Marco, N.; Zhou, H.; Chen, Q.; Sun, P.; Liu, Z.; Meng, L.; Yao, E.-P.; Liu, Y.; Schiffer, A.; Yang, Y. Guanidinium: A Route to Enhanced Carrier Lifetime and Open-Circuit Voltage in

Hybrid Perovskite Solar Cells. *Nano Letters* **2016**, *16*, 1009-1016, doi:10.1021/acs.nanolett.5b04060.

43. Jana, M.K.; Song, R.; Liu, H.; Khanal, D.R.; Janke, S.M.; Zhao, R.; Liu, C.; Valy Vardeny, Z.; Blum, V.; Mitzi, D.B. Organic-to-inorganic structural chirality transfer in a 2D hybrid perovskite and impact on Rashba-Dresselhaus spin-orbit coupling. *Nature Communications* **2020**, *11*, 4699, doi:10.1038/s41467-020-18485-7.
44. Ramakrishnan, S.; Li, H.; Xu, Y.; Shin, D.; Dursun, I.; Cotlet, M.; Zhang, Y.; Yu, Q. Ruddlesden–Popper Perovskites with Narrow Phase Distribution for Air-Stable Solar Cells. *Solar RRL* **2022**, *6*, 2200490, doi:https://doi.org/10.1002/solr.202200490.
45. Ma, J.; Fang, C.; Chen, C.; Jin, L.; Wang, J.; Wang, S.; Tang, J.; Li, D. Chiral 2D Perovskites with a High Degree of Circularly Polarized Photoluminescence. *ACS Nano* **2019**, *13*, 3659-3665, doi:10.1021/acsnano.9b00302.
46. Roknuzzaman, M.; Zhang, C.; Ostrikov, K.; Du, A.; Wang, H.; Wang, L.; Tesfamichael, T. Electronic and optical properties of lead-free hybrid double perovskites for photovoltaic and optoelectronic applications. *Scientific Reports* **2019**, *9*, 718, doi:10.1038/s41598-018-37132-2.
47. Yu, G.; Lin, F.; Zhou, K.; Fang, S.; Shi, Y.; Liu, W.; Hu, H.; Ma, B.; Lin, H. One-Dimensional Organic–Metal Halide with Highly Efficient Warm White-Light Emission and Its Moisture-Induced Structural Transformation. *Chemistry of Materials* **2021**, *33*, 5668-5674, doi:10.1021/acs.chemmater.1c01219.
48. Yu, J.; Li, M.; Lv, Y.; Liao, B.; Tan, G.; Zou, J.; Liu, X.; Han, Y.; Li, L. Second-Harmonic-Generation Circular-Dichroism in Chiral Perovskite Single Crystals Enhanced by Self-Trapped Excitonic State. *Advanced Functional Materials* **2026**, *36*, e08904, doi:https://doi.org/10.1002/adfm.202508904.
49. Lee, K.S.; Park, D.Y.; Jeong, M.S.; Kim, E.K. Analysis on the defect states of $FA_xMA_{1-x}PbI_3$ perovskite single crystals grown by inverse-temperature crystallization. *Applied Physics A* **2024**, *130*, 393.
50. Gogoi, B.; Yerramilli, A.; Luboowa, K.M.; Tagbor, E.; Alford, T. Fabrication of triple cation perovskite solar cells using different post-spin coating anti-solvent treatments. *Journal of Materials Science: Materials in Electronics* **2022**, *33*, 21161-21171.
51. Reddy, V.; Maniyarasu, S.; Battula, R.K.; Bhaskar, P.U.; Ramasamy, E.; Veerappan, G. Temperature dependence of $MAPbI_3$ films by quasi-vapor deposition technique and impact on photovoltaic performance and stability of perovskite solar cells. *Journal of Alloys and Compounds* **2021**, *888*, 161448.
52. Xue, W.; Zhang, X.; Zhu, W.; Zhang, X.; Wang, W.; Peng, L.; Ma, X.; Li, Y. Large-scale heterogeneous synthesis of monodisperse high performance colloidal $CsPbBr_3$ nanocrystals. *Fundamental Research* **2024**, *4*, 1137-1146.
53. Heinze, K.L.; Schulz, T.; Scheer, R.; Pistor, P. Structural Evolution of Sequentially Evaporated (Cs, FA) $Pb(I, Br)_3$ Perovskite Thin Films via In Situ X-Ray Diffraction. *physica status solidi (a)* **2024**, *221*, 2300690.

54. Ng, C.K.; Yin, W.; Li, H.; Jasieniak, J.J. Scalable synthesis of colloidal $CsPbBr_3$ perovskite nanocrystals with high reaction yields through solvent and ligand engineering. *Nanoscale* **2020**, *12*, 4859-4867.
55. Song, K.; Li, Q.; Guo, H.; Hu, Q.; Li, Z.; Li, F.; Fan, S.; Xu, Z. Composition and electrical properties characterization of a 5″ diameter PIN-PMN-PT single crystal by the modified Bridgman method. *Journal of Alloys and Compounds* **2021**, *851*, 156145, doi:https://doi.org/10.1016/j.jallcom.2020.156145.
56. Huang, L.; Lu, H.; Liu, X.; Song, Z.; Su, J.; Li, Z.; Song, S.; Liu, L. Self-catalyzed Growth and Optoelectronic Properties of High-Quality $CsPbBr_3$ and $CsPbI_3$ Nanowires Based on Chemical Vapor Deposition. *Journal of Physics: Conference Series* **2024**, *2809*, 012037, doi:10.1088/1742-6596/2809/1/012037.
57. Fievez, M. Slot-die coating of hybrid perovskite: material study and integration into photovoltaic devices. Université Grenoble Alpes [2020], Nanyang Technological University (Singapour), 2021. English. ⟨NNT: 2021GRALI051⟩.
58. Cheng, Q.; You, S.; Zhang, W.; Xie, M.; Yue, T.; Tian, C.; Zhang, H.; Wei, Z.; Li, X.; Zhang, Y.; et al. Single Crystal Seed Induced Epitaxial Growth Stabilizes α-$FAPbI_3$ in Perovskite Solar Cells. *Nano Letters* **2024**, *24*, 5308-5316, doi:10.1021/acs.nanolett.4c00993.
59. Dagar, J.; Fenske, M.; Al-Ashouri, A.; Schultz, C.; Li, B.; Köbler, H.; Munir, R.; Parmasivam, G.; Li, J.; Levine, I.; et al. Compositional and Interfacial Engineering Yield High-Performance and Stable p-i-n Perovskite Solar Cells and Mini-Modules. *ACS Applied Materials & Interfaces* **2021**, *13*, 13022-13033, doi:10.1021/acsami.0c17893.
60. Yang, G.; Ni, Z.; Yu, Z.J.; Larson, B.W.; Yu, Z.; Chen, B.; Alasfour, A.; Xiao, X.; Luther, J.M.; Holman, Z.C.; et al. Defect engineering in wide-bandgap perovskites for efficient perovskite–silicon tandem solar cells. *Nature Photonics* **2022**, *16*, 588-594, doi:10.1038/s41566-022-01033-8.
61. Xing, Z.; Jin, G.; Du, Q.; Pang, P.; Liu, T.; Shen, Y.; Zhang, D.; Yu, B.; Liang, Y.; Yang, D.; et al. Ions-induced Assembly of Perovskite Nanocomposites for Highly Efficient Light-Emitting Diodes with EQE Exceeding 30. *Adv Mater* **2024**, *36*, e2406706, doi:10.1002/adma.202406706.
62. Ren, M.; Cao, S.; Zhao, J.; Zou, B.; Zeng, R. Advances and Challenges in Two-Dimensional Organic-Inorganic Hybrid Perovskites Toward High-Performance Light-Emitting Diodes. *Nanomicro Lett* **2021**, *13*, 163, doi:10.1007/s40820-021-00685-5.
63. Bhuvaneswari, P.; Sriramalakshmi, P. Lead-Free p-n Homojunction Cs-Doped and Pure $FASnI_3$-based perovskite solar cells–a performance analysis using SCAPS 1D simulator. *Results in Engineering* **2025**, *26*, 104779, doi:https://doi.org/10.1016/j.rineng.2025.104779.
64. Jiang, N.; Ma, G.; Zhu, M.; Song, D.; Qiao, B.; Liang, Z.; Xu, Z.; Zhao, S. Manipulating Phase and Defect Distribution of Quasi-2D Perovskites via a Synergistic Strategy for Enhancing the Performance of Blue Light-Emitting Diodes. *ACS Applied Materials & Interfaces* **2025**, *17*, 8024-8035, doi:10.1021/acsami.4c21188.
65. Furlan, F.; Moreno-Naranjo, J.M.; Gasparini, N.; Feldmann, S.; Wade, J.; Fuchter, M.J. Chiral materials and mechanisms for circularly polarized light-emitting diodes. *Nature Photonics* **2024**, *18*, 658-668, doi:10.1038/s41566-024-01408-z.

66. Yang, H.; Sun, B.; Guan, J.; Wu, S.-D.; Tan, X.-Y.; Wang, P.; Xu, J.; Zhang, H.-L. High Circularly Polarized Luminescence Dissymmetry Factor and Efficient Chiral Second Harmonic Generation in Chiral Hybrid Lead-Bromide Perovskites. *Advanced Optical Materials* **2025**, *13*, 2500394, doi:https://doi.org/10.1002/adom.202500394.
67. Du, L.; Zhou, Q.; He, Q.; Liu, Y.; Shen, Y.; Lv, H.; Sheng, L.; Cheng, T.; Yang, H.; Wan, L.; et al. Efficient Circularly Polarized Luminescence and Bright White Emission from Hybrid Indium-Based Perovskites via Achiral Building Blocks. *Advanced Functional Materials* **2024**, *34*, 2315676, doi:https://doi.org/10.1002/adfm.202315676.
68. Li, C.; Wang, H.; Wang, F.; Li, T.; Xu, M.; Wang, H.; Wang, Z.; Zhan, X.; Hu, W.; Shen, L. Ultrafast and broadband photodetectors based on a perovskite/organic bulk heterojunction for large-dynamic-range imaging. *Light: Science & Applications* **2020**, *9*, 31, doi:10.1038/s41377-020-0264-5.
69. Chai, Y.; Jiang, C.; Hu, X.; Han, J.; Wang, Y.; Yang, W.; Li, C.; Zeng, H.; Li, X. Homogeneous Bridging Induces Compact and Scalable Perovskite Thick Films for X-Ray Flat-Panel Detectors. *Small* **2023**, *19*, 2305357, doi:https://doi.org/10.1002/smll.202305357.
70. Chen, C.; Gao, L.; Gao, W.; Ge, C.; Du, X.; Li, Z.; Yang, Y.; Niu, G.; Tang, J. Circularly polarized light detection using chiral hybrid perovskite. *Nature Communications* **2019**, *10*, 1927, doi:10.1038/s41467-019-09942-z.
71. Zhang, X.; Xu, Y.; Alphenaar, A.N.; Ramakrishnan, S.; Zhang, Y.; Babatunde, A.J.; Yu, Q. Self-Powered Circularly Polarized Light Detection Enabled by Chiral Two-Dimensional Perovskites with Mixed Chiral–Achiral Organic Cations. *ACS Nano* **2024**, *18*, 14605-14616, doi:10.1021/acsnano.4c02588.
72. Ishii, A.; Miyasaka, T. Direct detection of circular polarized light in helical 1D perovskite-based photodiode. *Sci Adv* **2020**, *6*, doi:10.1126/sciadv.abd3274.
73. Zhou, C.; Tarasov, A.B.; Goodilin, E.A.; Chen, P.; Wang, H.; Chen, Q. Recent strategies to improve moisture stability in metal halide perovskites materials and devices. *Journal of Energy Chemistry* **2022**, *65*, 219-235, doi:https://doi.org/10.1016/j.jechem.2021.05.035.
74. Abdelmageed, G.; Mackeen, C.; Hellier, K.; Jewell, L.; Seymour, L.; Tingwald, M.; Bridges, F.; Zhang, J.Z.; Carter, S. Effect of temperature on light induced degradation in methylammonium lead iodide perovskite thin films and solar cells. *Solar Energy Materials and Solar Cells* **2018**, *174*, 566-571, doi:https://doi.org/10.1016/j.solmat.2017.09.053.
75. Ruellou, J.; Courty, M.; Sauvage, F. Thermal and Photo-Degradation Study of α-FAPbI3-Based Perovskite Using In Situ X-Ray Diffraction. *Advanced Functional Materials* **2023**, *33*, 2300811, doi:https://doi.org/10.1002/adfm.202300811.
76. DuBose, J.T.; Kamat, P.V. Hole Trapping in Halide Perovskites Induces Phase Segregation. *Accounts of Materials Research* **2022**, *3*, 761-771, doi:10.1021/accountsmr.2c00076.
77. Fu, W.; Liu, H.; Shi, X.; Zuo, L.; Li, X.; Jen, A.K.-Y. Tailoring the Functionality of Organic Spacer Cations for Efficient and Stable Quasi-2D Perovskite Solar Cells. *Advanced Functional Materials* **2019**, *29*, 1900221, doi:https://doi.org/10.1002/adfm.201900221.

78. Cao, C.; Tao, Y.; Yang, Q.; Yu, H.; Chen, Y.; Meng, Q.; Ye, J.; Pan, X. Bilayer interfacial engineering with PEAI/OAI for synergistic defect passivation in high-performance perovskite solar cells. *Journal of Semiconductors* **2025**, *46*, 052805, doi:10.1088/1674-4926/25030046.
79. Castro-Hermosa, S.; Top, M.; Dagar, J.; Fahlteich, J.; Brown, T.M. Quantifying Performance of Permeation Barrier—Encapsulation Systems for Flexible and Glass-Based Electronics and Their Application to Perovskite Solar Cells. *Advanced Electronic Materials* **2019**, *5*, 1800978, doi:https://doi.org/10.1002/aelm.201800978.
80. Long, G.; Sabatini, R.; Saidaminov, M.I.; Lakhwani, G.; Rasmita, A.; Liu, X.; Sargent, E.H.; Gao, W. Chiral-perovskite optoelectronics. *Nature Reviews Materials* **2020**, *5*, 423-439, doi:10.1038/s41578-020-0181-5.
81. Lu, H.; Xiao, C.; Song, R.; Li, T.; Maughan, A.E.; Levin, A.; Brunecky, R.; Berry, J.J.; Mitzi, D.B.; Blum, V.; et al. Highly Distorted Chiral Two-Dimensional Tin Iodide Perovskites for Spin Polarized Charge Transport. *Journal of the American Chemical Society* **2020**, *142*, 13030-13040, doi:10.1021/jacs.0c03899.
82. Liu, Q.; Ren, H.; Wei, Q.; Li, M. Multifunctional Chiral Halide Perovskites: Advancing Chiro-Optics, Chiro-Optoelectronics, and Spintronics. *Advanced Science* **2025**, *12*, e09155, doi:https://doi.org/10.1002/advs.202509155.
83. Yao, L.; Zhang, Q.; Li, M.; Chen, C.; Gu, H.; Liu, S.; Long, G.; Liu, F.; Yang, W.; Tang, J. Amplification of Chirality in Self-Assembled Chiral Perovskite Superstructure Films. *Journal of the American Chemical Society* **2025**, *147*, 36420-36427, doi:10.1021/jacs.5c10609.
84. Panagiotopoulou, C.; Liu, S.; Pittrich, J.; Iglev, H.; Deschler, F.; Kartouzian, A. Chiroptical Amplification Beyond Enantiopurity in Chiral Films. *Advanced Optical Materials* **2025**, *13*, e01895, doi:https://doi.org/10.1002/adom.202501895.

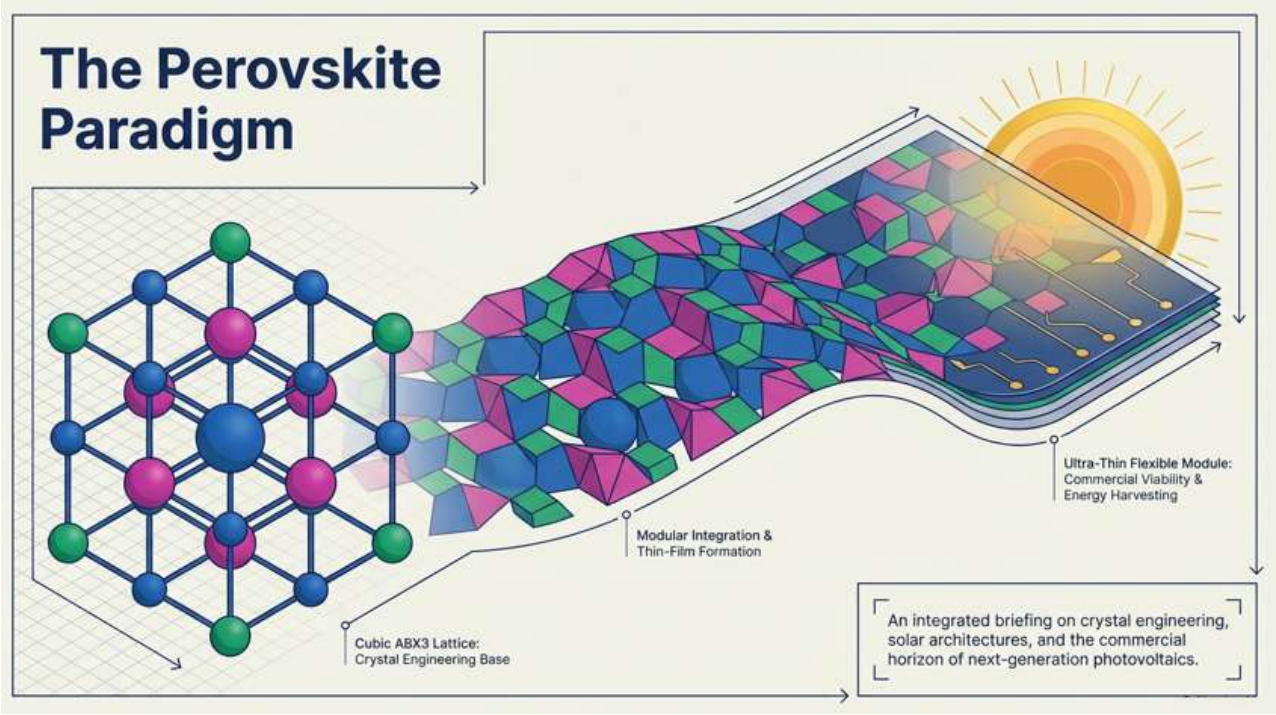

Graphical Abstract